Electronic Supplementary Information for

Amorphous and outstandingly stable $Ni(OH)_2 \cdot 0.75H_2O$@$Ni(OH)_2$/FeOOH heterojunction nanosheets for efficient oxygen evolution performance

Tingyi Huang‡, Yawen Liu‡, Ziyu Zhao, Yuchan Liu, Rongkai Ye * and Jianqiang Hu*

School of Chemistry and Chemical Engineering, Key Lab of Fuel Cell Technology of Guangdong Province, South China University of Technology, Guangzhou, 510640, P. R. China. E-mail: jqhusc@scut.edu.cn, kairyscut@scut.edu.cn

‡ Tingyi Huang and Yawen Liu contributed equally to this work.

1. Experimental section

1.1 Chemicals

Nickel nitrate hexahydrate ($Ni(NO_3)_2·6H_2O$, 98%), ferric chloride hexahydrate ($FeCl_3·6H_2O$, 98%), urea (CH_4N_2O, 98%), ammonium fluoride (NH_4F, 99%), sodium hydroxide (NaOH) and commercial ruthenium dioxide (RuO_2, 99.9%) were purchased from Aladdin (Shanghai, China), and used without any further purification. The solutions in present work were prepared by ultra-pure water (>18.0 MΩ·cm).

1.2 Preparation of electrocatalysts

1.2.1 Preparation of $Ni(NO_3)_2·0.75H_2O$@$Ni(OH)_2$ nanosheets

Ni foam (NF) was cut into rectangular pieces (3*2 cm^2) and then carefully pretreated through complying following steps before each experiment: firstly, the NF slices were ultrasonicated in 3.0 M HCl for 20 min to remove oxide layer on surface. Then the NF slices were successively ultrasonicated in acetone, ethanol and water for 10 min, respectively.

0.491 g $Ni(NO_3)_2·6H_2O$, 0.451 g urea and 0.111 g NH_4F were dissolved in 30 mL ultrapure water. Then, a piece of treated NF was completely immersed into the solution, and the reaction was heated in a sealed stainless steel autoclave at 100 °C for 6 h. After the reaction, the autoclave was cooled naturally to room temperature. Subsequently, the NF was removed from the react solution and washed three times with water and ethanol. The as-prepared electrocatalyst was dried under vacuum at 60 °C to obtain the $Ni(OH)_2·0.75H_2O$@$Ni(OH)_2$ nanosheets *in situ* grown on NF, which would be cut into 1*1 cm^2 for further use.

1.2.2 Preparation of the $Ni(OH)_2·0.75H_2O$@$Ni(OH)_2$/FeOOH nanosheets

Amorphous FeOOH was electrodeposited on the surface of as-prepared $Ni(OH)_2·0.75H_2O$@$Ni(OH)_2$ nanosheets through using Pt sheet and saturated calomel electrode as counter electrode and reference electrode, respectively. The electrodeposition was performed in 0.1 M $Fe(NO_3)_3$ aqueous solution at -1.0 V (*vs*. saturated calomel electrode).

1.2.3 Preparation of RuO_2/NF

The commercial RuO_2 (10 mg) was dispersed into a mixture of 980 μL ethanol and 20 μL Nafion (5%), and the mixture was ultrasonicated for 30 min to form homogeneous ink. Then, a certain amount ink was loaded onto nickel foam and dried at room temperature. The loading amount of RuO_2 on the 1*1 cm^2 NF was about 2.5 $mg \cdot cm^{-2}$, which was the same amount with the as-prepared electrocatalysts.

1.3 Characterization

The morphology and structure of the samples were characterized by scanning electron microscopy (SEM, Hitachi SU8010, 5kV) and transmission electron microscopy (TEM, JEOL, JEM-1400, 120 kV). The crystallinity and purity of the materials was evaluated qualitatively by thin film powder X-ray diffraction (XRD, Bruker, D8 Advance, Germany) equipped with a Cu Kα radiation source (λ=1.5406 Å), and the test conditions were set as 2θ range from 5° to 50° at scanning rate of $5° \cdot min^{-1}$. The surface properties of the products were analyzed with X-ray photoelectron spectroscopy (XPS, Nexsa, Thermo Fisher Scientific, America) with a Mg Kα X-ray source. The content of Ni and Fe in different specimens was determined by inductively couple plasma-mass spectrometer (ICP-MS, iCAP Qc, Thermo Fisher Scientific).

1.4 Electrochemical measurements

Electrochemical measurements were performed on a CHI 760E electrochemistry workstation with a three-electrode system. The saturated Ag/AgCl and Pt plate electrode were used as the reference and counter electrode, respectively. The as-prepared catalysts on NF were used as working electrodes. The measured potentials were converted to reversible hydrogen electrode (RHE), $E_{RHE} = E_{Ag/AgCl} + 0.21 + 0.059 \times pH$. Linear sweep voltammetry (LSV) curves were recorded in 1.0 M KOH (pH=13.4) aqueous solutions with 95% *iR*-compensation at a scan rate of 2 $mV \cdot s^{-1}$. Tafel slopes were calculated by linear regression using the equation $\eta = b \cdot \log|j| + a$, where η (V) is the overpotential, j is the current density ($mA \cdot cm^{-2}$), respectively. The electrochemically active surface areas were investigated by double-layer capacitance (C_{dl}) in the potential range from 0-0.1 V vs. $E_{Ag/AgCl}$ with

different scan rates (20, 40, 80, 120, 160 and 200 $mV \cdot s^{-1}$). The electrochemical impedance spectroscopy (EIS) was measured in 1.0 M KOH aqueous solutions with a frequency range from 10^5 to 0.01 Hz at 1.45 V *vs.* RHE. The stability measurements were conducted in 1 M KOH solution at room temperature and the current density of 100 $mA \cdot cm^{-2}$.

2. Supplementary figures

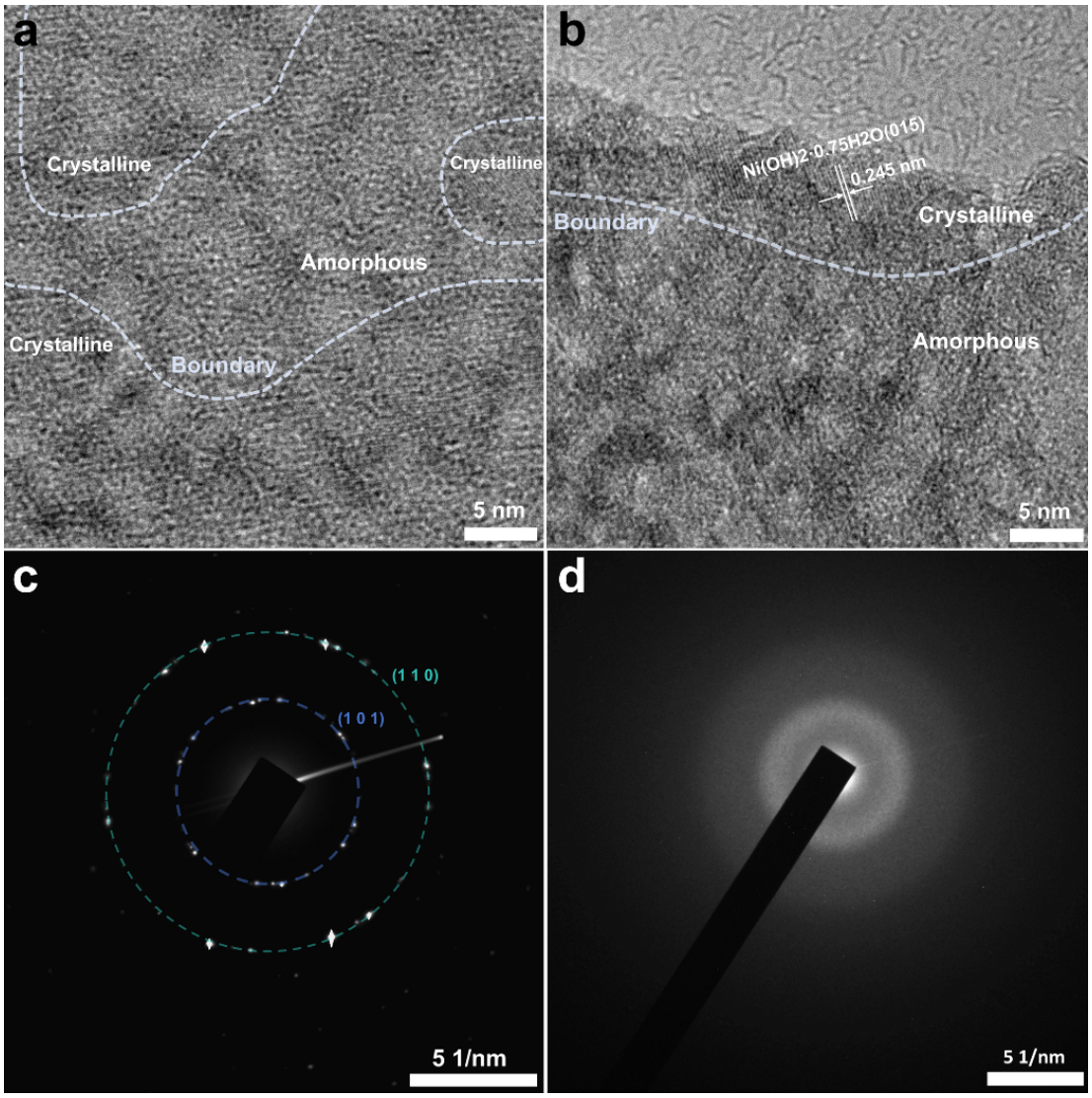

Fig. S1 (a,b) HRTEM images and (c) selected area electron diffraction pattern of $Ni(OH)_2 \cdot 0.75H_2O$@$Ni(OH)_2$/FeOOH nanosheets. (d) Selected area electron diffraction pattern of FeOOH/NF.

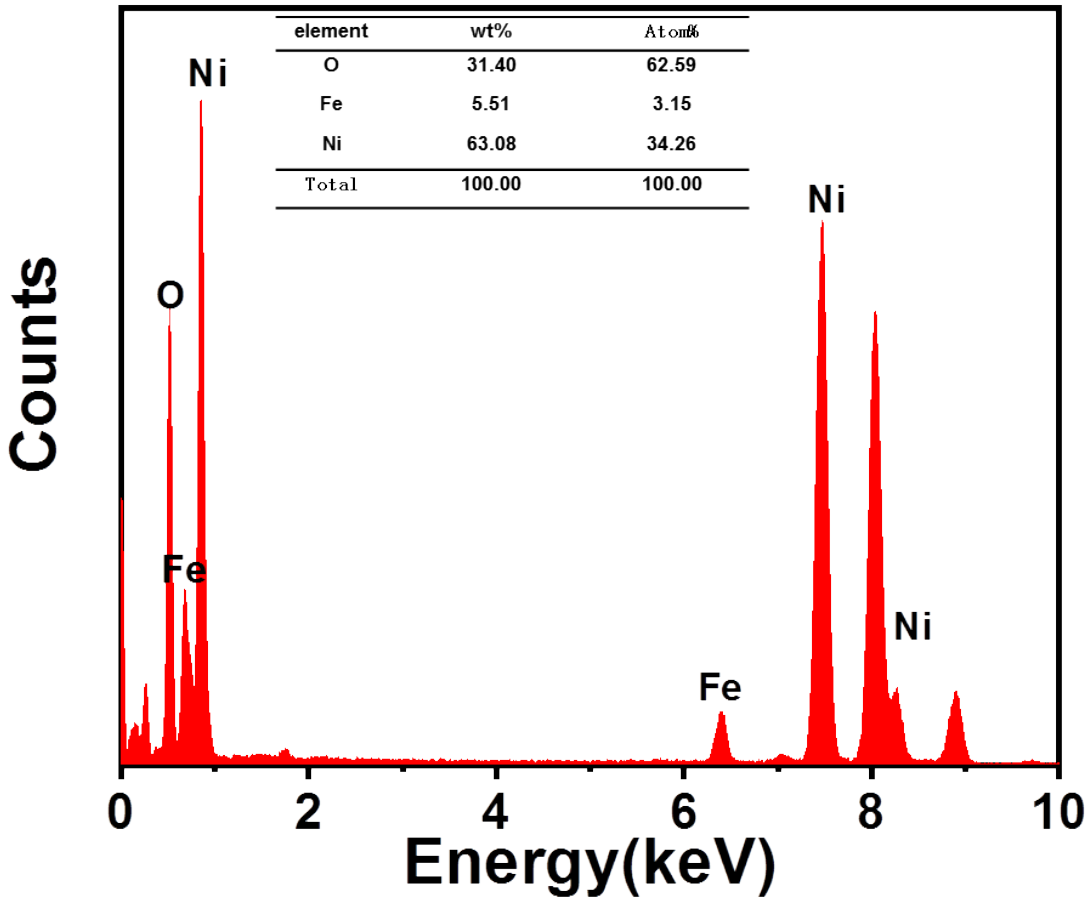

Fig. S2 EDX pattern of the $Ni(OH)_2 \cdot 0.75H_2O$@$Ni(OH)_2$/FeOOH heterojunction nanosheets fabricated by the present method.

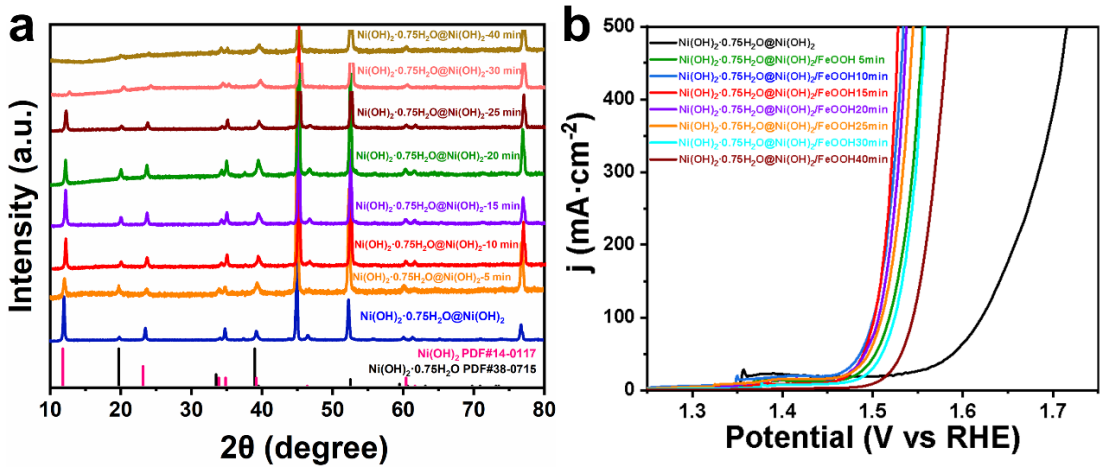

Fig. S3 (a) XRD patterns and (b) OER performance in 1.0 M KOH of the $Ni(OH)_2{\cdot}0.75H_2O$@$Ni(OH)_2$/FeOOH nanosheets prepared using different time of electrodeposition.

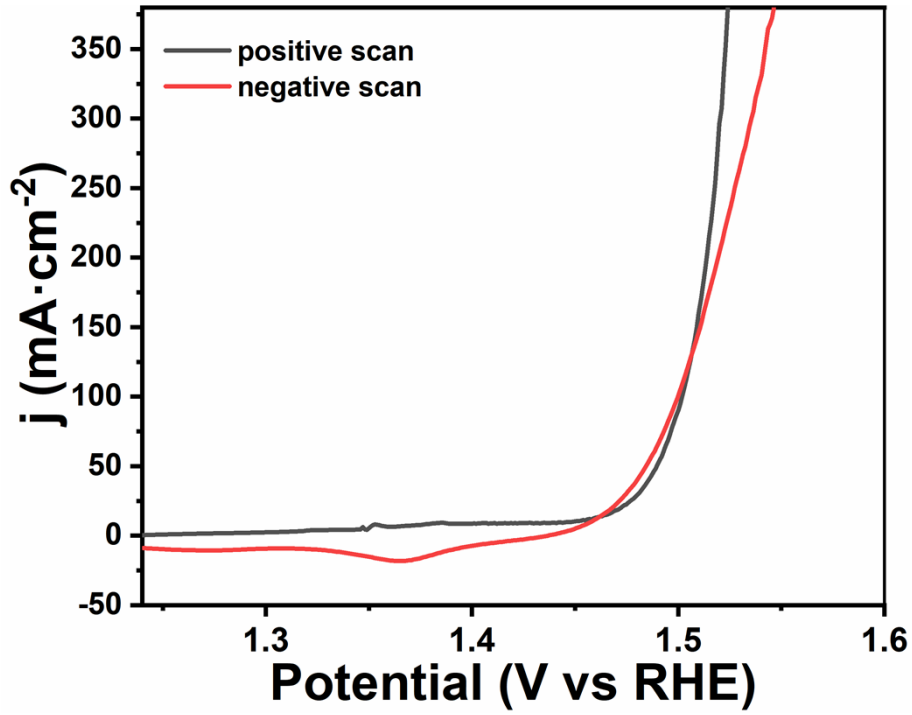

Fig. S4 The positive and negative LSV curves of the $Ni(OH)_2 \cdot 0.75H_2O$@$Ni(OH)_2$/FeOOH nanosheets in 1.0 M KOH.

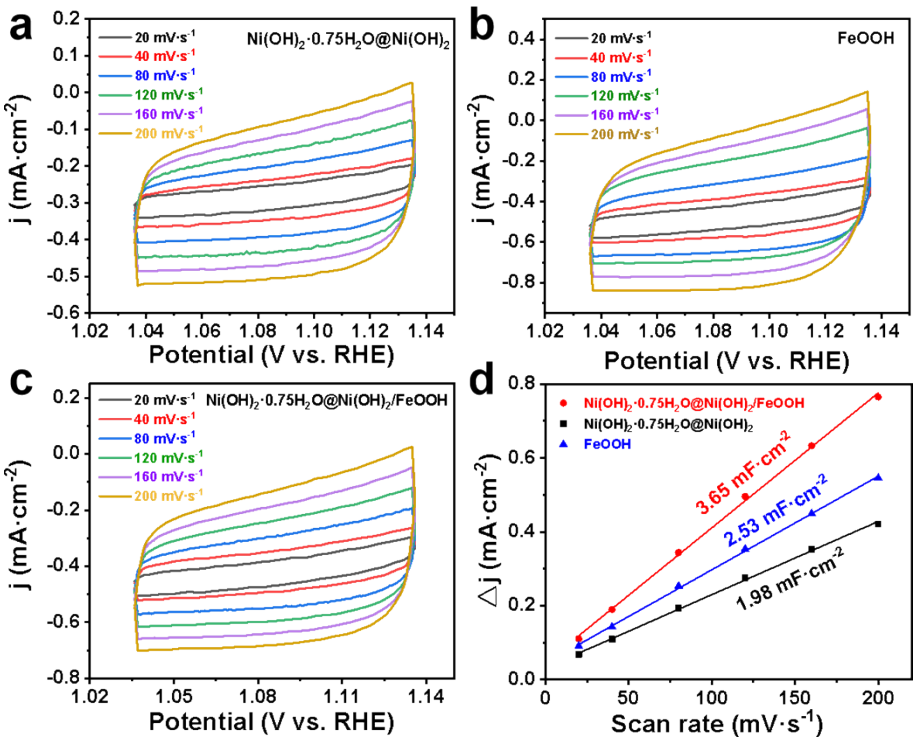

Fig. S5 CV curves of (a) $Ni(OH)_2 \cdot 0.75H_2O@Ni(OH)_2$, (b) FeOOH and (c) $Ni(OH)_2 \cdot 0.75H_2O@Ni(OH)_2$/FeOOH nanosheets. (d) Plots of current density difference (Δj) at 1.08 V (*vs.* RHE) against scan rates for calculation of double layer capacitance (C_{dl}).

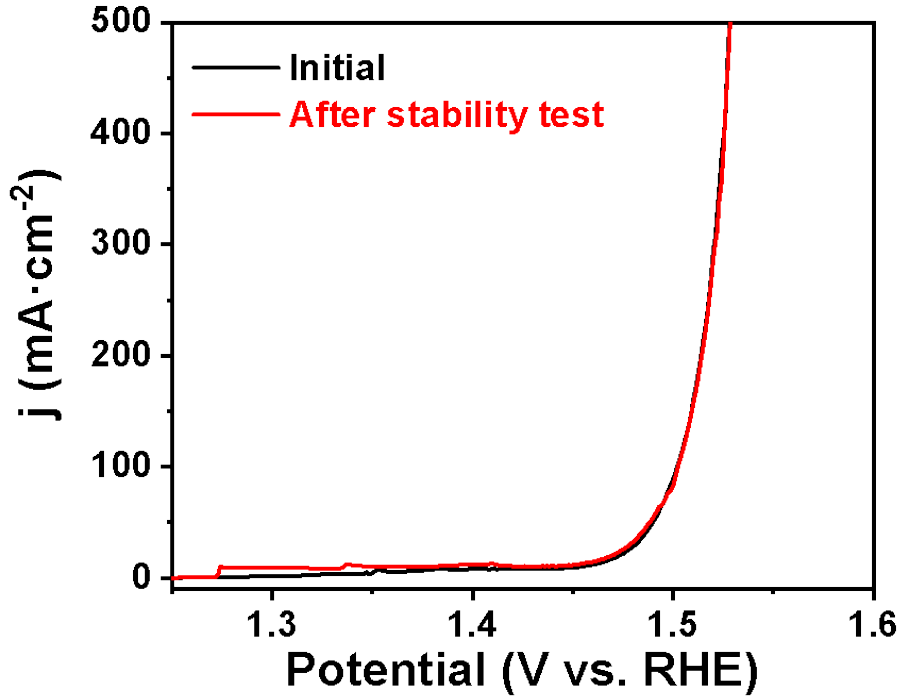

Fig. S6 OER performance of the $Ni(OH)_2 \cdot 0.75H_2O$@$Ni(OH)_2$/FeOOH nanosheets before and after stability measurement in 1.0 M KOH.

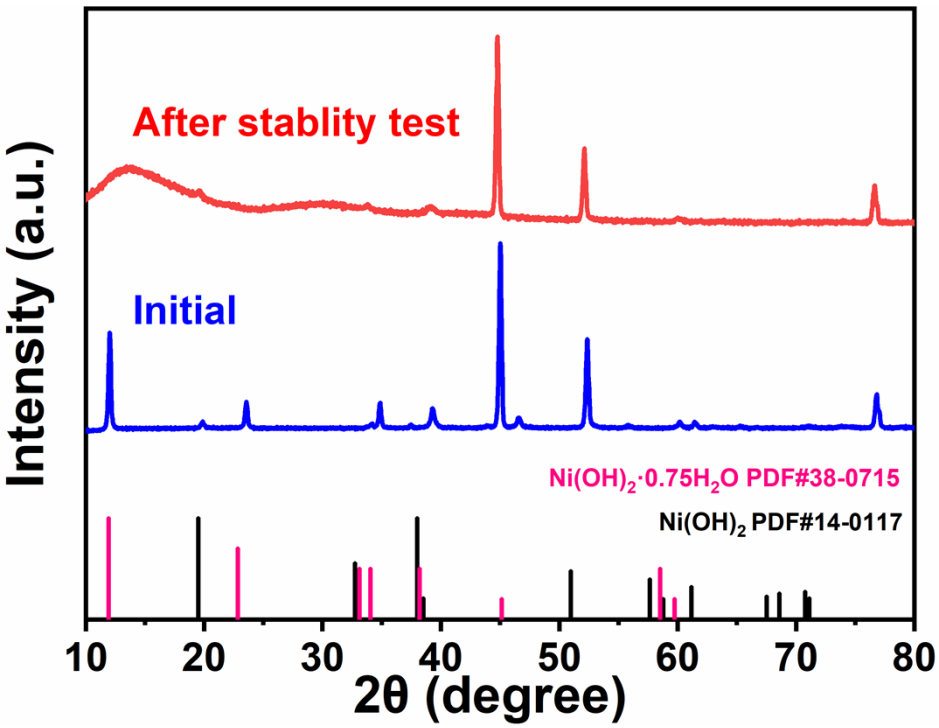

Fig. S7 XRD patterns of the $Ni(OH)_2 \cdot 0.75H_2O$@$Ni(OH)_2$/FeOOH nanosheets before and after stability measurement for100 h.

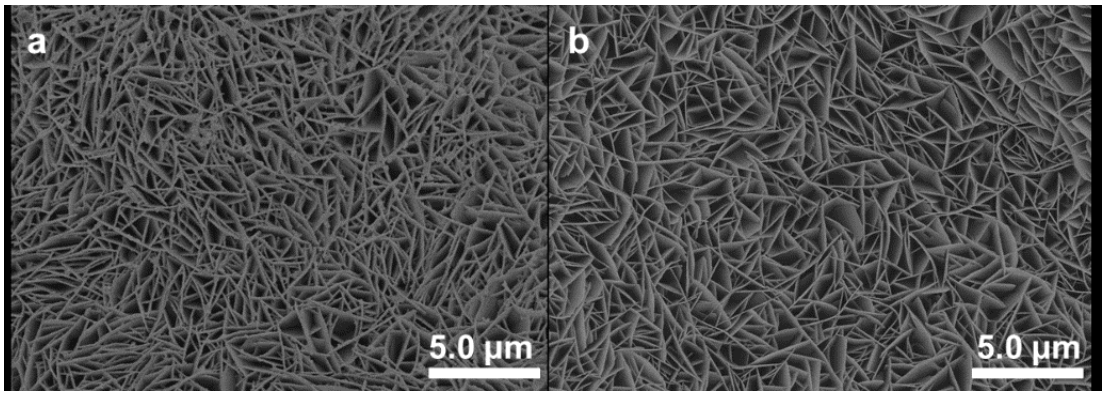

Fig. S8 SEM images of $Ni(OH)_2 \cdot 0.75H_2O$@$Ni(OH)_2$/FeOOH (a) before and (b) after stability measurements.

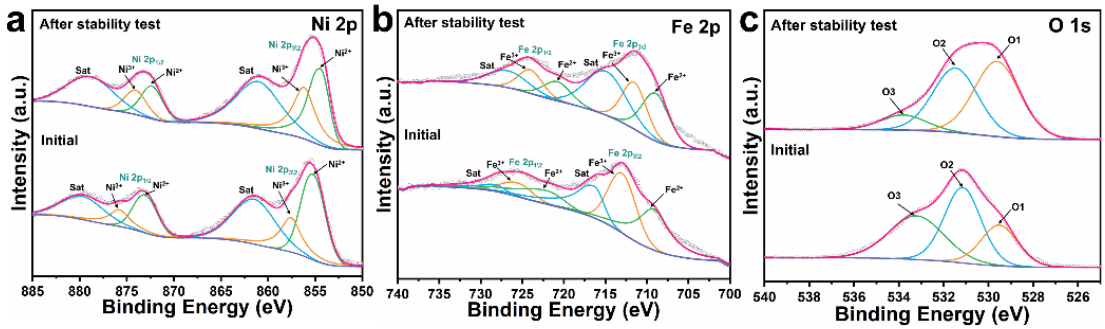

Fig. S9 XPS high-resolution spectra of (a) Ni 2p, (b) Fe 2p and (c) O 1s of the $Ni(OH)_2 \cdot 0.75H_2O$@$Ni(OH)_2$/FeOOH nanosheets before and after stability measurements.

Table S1 EIS results of different electrocatalysts.

Catalysts	Solution impedance R_s (Ω)	Charge transfer impedance R_{ct} (Ω)
FeOOH	1.94	1.22
$Ni(OH)_2 \cdot 0.75H_2O@Ni(OH)_2$	1.98	13.35
$Ni(OH)_2 \cdot 0.75H_2O@Ni(OH)_2$/FeOOH	1.97	0.43

Table S2 Comparison of OER activities of art non-noble-metal electrocatalysts.

Catalyst	Overpotential (mV)	Tafel slope (mV dec^{-1})	Substrates	Refs.
$Ni(OH)_2 \cdot 0.75H_2O$@$Ni(OH)_2$/FeOOH	η_{50}=256 η_{100}=270	44	Ni foam	**This work**
(Ni, Fe)Se@NiFe-LDH	H_{100}=253	42	Ni foam	1
$NiFe_3Nb_2$-OH	η_{100}=294	47	Ni foam	2
NiFe-HD/pre-NF	η_{100}=256	81	Ni foam	3
CoP/P-NiO/NF	η_{100}=265	101.8	Ni foam	4
$NiCo_{1.09}$BDC-$Fc_{0.25}$/NF	η_{100}=278	43	Ni foam	5
W-Ni_3S_2/Ni_7S_6	H_{100}=202	55	Ni foam	6
Ni–Fe–Se/NF	η_{100}=222	39	Ni foam	7
Fe_4Ni-Se/NF	η_{10}=207	36.7	Ni foam	8
$Ni(OH)_2$-Fe H-STs-Ni_3Fe_1/NF	η_{10}=200	53	Ni foam	9
$Fe_{0.5}Ni_{0.5}$Pc-CP	η_{10}=317	116	carbon paper	10
$NiFe_{0.05}$-N-CP	η_{10}=238	76	carbon paper	11
α-$Ni(OH)_2$ thin films	H_{10}=310	42.6	GCE	12
$Ni(OH)_2$ NPs@CSZ	η_{10}=212	64.2	GCE	13
$Ni_{0.25}Co_{0.75}(OH)_2$	η_{10}=352	72	GCE	14
Ni–N@5min nanoclusters	η_{100}=294	42.5	GCE	15

References

1 J. Hu, Y. Q. Liang, S. L. Wu, Z. Y. Li, C. S. Shi, S. Y. Luo, H. J. Sun, S. L. Zhu and Z. D. Cui, *Mater. Today Nano*, 2022, **17**, 100150.

2 D. Hu, X. Wang, X. Chen, Y. Wang, A. N. Hong, J. Zhong, X. Bu, P. Feng and T. Wu, *J. Mater. Chem. A*, 2020, **8**, 11255–11260.

3 B. Wu, Z. Yang, X. Dai, X. Yin, Y. Gan, F. Nie, Z. Ren, Y. Cao, Z. Li and X. Zhang, *Dalton Trans.*, 2021, **50**, 12547–12554.

4 F. Nie, Z. Yang, X. Dai, Z. Ren, X. Yin, Y. Gan, B. Wu, Y. Cao, R. Cai and X. Zhang, *J. Colloid Interface Sci.*, 2022, **621**, 213–221.

5 Q. Liang, Y. Liu, Z. Xue, Z. Zhao, G. Li and J. Hu, *Chem. Commun.*, 2022, **58**, 6966–6969.

6 Z. Xue, Y. Liu, Q. Liu, Y. Zhang, M. Yu, Q. Liang, J. Hu and G. Li, *J. Mater. Chem. A*, 2022, **10**, 3341–3345.

7 X. Yi, X. He, F. Yin, B. Chen, G. Li and H. Yin, *Dalton Trans.*, 2020, **49**, 6764–6775.

8 C. Jin, M. Hou, X. Li, D. Liu, D. Qu, Y. Dong, Z. Xie and C. Zhang, *J. Electroanal. Chem.*, 2022, **906**, 116014.

9 Y. Ding, B.-Q. Miao, Y. Zhao, F.-M. Li, Y.-C. Jiang, S.-N. Li and Y. Chen, *Chin. J. Catal.*, 2021, **42**, 271–278.

10 D. Qi, X. Chen, W. Liu, C. Liu, W. Liu, K. Wang and J. Jiang, *Inorg. Chem. Front.*, 2020, **7**, 642–646.

11 Y. Xu, Z. Cheng, J. Jiang, J. Du and Q. Xu, *Chem. Commun.*, 2021, **57**, 13170–13173.

12 S. Tao, Q. Wen, W. Jaegermann and B. Kaiser, *ACS Catal.*, 2022, **12**, 1508–1519.

13 D. Hu, X. Wang, X. Chen, Y. Wang, A. N. Hong, J. Zhong, X. Bu, P. Feng and T. Wu, *J. Mater. Chem. A*, 2020, **8**, 11255–11260.

14 Y. Wang, C. Yang, Y. Huang, Z. Li, Z. Liang and G. Cao, *J. Mater. Chem. A*, 2020, **8**, 6699–6708.

15 T. Yu, Y. Hou, P. Shi, Y. Yang, M. Chen, W. Zhou, Z. Jiang, X. Luo, H. Zhou and C. Yuan, *Inorg. Chem.*, 2022, **61**, 2360–2367.